



# CHORUS

This is the accepted manuscript made available via CHORUS. The article has been published as:

## Observation of $D^0 \rightarrow \rho^0 \gamma$ and Search for CP Violation in Radiative Charm Decays

T. Nanut *et al.* (Belle Collaboration)

Phys. Rev. Lett. **118**, 051801 — Published 31 January 2017

DOI: [10.1103/PhysRevLett.118.051801](https://doi.org/10.1103/PhysRevLett.118.051801)

# Observation of $D^0 \rightarrow \rho^0 \gamma$ and search for $CP$ violation in radiative charm decays

T. Nanut,<sup>27</sup> A. Zupanc,<sup>38,27</sup> I. Adachi,<sup>16,12</sup> H. Aihara,<sup>73</sup> S. Al Said,<sup>67,32</sup> D. M. Asner,<sup>58</sup> V. Aulchenko,<sup>5,57</sup>  
T. Aushev,<sup>46</sup> R. Ayad,<sup>67</sup> V. Babu,<sup>68</sup> I. Badhrees,<sup>67,31</sup> A. M. Bakich,<sup>66</sup> V. Bansal,<sup>58</sup> P. Behera,<sup>22</sup> V. Bhardwaj,<sup>19</sup>  
J. Biswal,<sup>27</sup> A. Bondar,<sup>5,57</sup> A. Bozek,<sup>53</sup> M. Bračko,<sup>41,27</sup> T. E. Browder,<sup>15</sup> D. Červenkov,<sup>6</sup> V. Chekelian,<sup>42</sup>  
A. Chen,<sup>50</sup> B. G. Cheon,<sup>14</sup> R. Chistov,<sup>37,45</sup> K. Cho,<sup>33</sup> S.-K. Choi,<sup>13</sup> Y. Choi,<sup>65</sup> D. Cinabro,<sup>78</sup> N. Dash,<sup>20</sup>  
S. Di Carlo,<sup>78</sup> Z. Doležal,<sup>6</sup> D. Dutta,<sup>68</sup> S. Eidelman,<sup>5,57</sup> H. Farhat,<sup>78</sup> J. E. Fast,<sup>58</sup> T. Ferber,<sup>9</sup> B. G. Fulsom,<sup>58</sup>  
V. Gaur,<sup>68</sup> N. Gabyshev,<sup>5,57</sup> A. Garmash,<sup>5,57</sup> R. Gillard,<sup>78</sup> P. Goldenzweig,<sup>29</sup> B. Golob,<sup>38,27</sup> K. Hayasaka,<sup>55</sup>  
H. Hayashii,<sup>49</sup> W.-S. Hou,<sup>52</sup> T. Iijima,<sup>48,47</sup> K. Inami,<sup>47</sup> G. Inguglia,<sup>9</sup> A. Ishikawa,<sup>71</sup> Y. Iwasaki,<sup>16</sup> W. W. Jacobs,<sup>23</sup>  
I. Jaegle,<sup>10</sup> D. Joffe,<sup>30</sup> K. K. Joo,<sup>7</sup> T. Julius,<sup>43</sup> A. B. Kaliyar,<sup>22</sup> K. H. Kang,<sup>35</sup> T. Kawasaki,<sup>55</sup> D. Y. Kim,<sup>63</sup>  
J. B. Kim,<sup>34</sup> K. T. Kim,<sup>34</sup> M. J. Kim,<sup>35</sup> S. H. Kim,<sup>14</sup> K. Kinoshita,<sup>8</sup> P. Kodyš,<sup>6</sup> S. Korpar,<sup>41,27</sup> P. Krokovny,<sup>5,57</sup>  
T. Kuhr,<sup>39</sup> R. Kulasiri,<sup>30</sup> A. Kuzmin,<sup>5,57</sup> Y.-J. Kwon,<sup>80</sup> J. S. Lange,<sup>11</sup> I. S. Lee,<sup>14</sup> C. H. Li,<sup>43</sup> L. Li,<sup>61</sup> Y. Li,<sup>77</sup>  
L. Li Gioi,<sup>42</sup> J. Libby,<sup>22</sup> D. Liventsev,<sup>77,16</sup> M. Lubej,<sup>27</sup> M. Masuda,<sup>72</sup> T. Matsuda,<sup>44</sup> D. Matvienko,<sup>5,57</sup>  
K. Miyabayashi,<sup>49</sup> H. Miyata,<sup>55</sup> R. Mizuk,<sup>37,45,46</sup> G. B. Mohanty,<sup>68</sup> H. K. Moon,<sup>34</sup> M. Nakao,<sup>16,12</sup> K. J. Nath,<sup>21</sup>  
M. Nayak,<sup>78,16</sup> N. K. Nisar,<sup>68,1</sup> S. Nishida,<sup>16,12</sup> S. Ogawa,<sup>70</sup> S. Okuno,<sup>28</sup> P. Pakhlov,<sup>37,45</sup> G. Pakhlova,<sup>37,46</sup>  
B. Pal,<sup>8</sup> C.-S. Park,<sup>80</sup> C. W. Park,<sup>65</sup> H. Park,<sup>35</sup> S. Paul,<sup>69</sup> T. K. Pedlar,<sup>40</sup> L. Pesántez,<sup>4</sup> R. Pestotnik,<sup>27</sup>  
M. Petrič,<sup>27</sup> L. E. Piilonen,<sup>77</sup> K. Prasanth,<sup>22</sup> C. Pulvermacher,<sup>16</sup> J. Rauch,<sup>69</sup> M. Ritter,<sup>39</sup> A. Rostomyan,<sup>9</sup>  
Y. Sakai,<sup>16,12</sup> S. Sandilya,<sup>8</sup> L. Santelj,<sup>16</sup> T. Sanuki,<sup>71</sup> Y. Sato,<sup>47</sup> V. Savinov,<sup>59</sup> T. Schlüter,<sup>39</sup> O. Schneider,<sup>36</sup>  
G. Schnell,<sup>2,18</sup> C. Schwanda,<sup>25</sup> A. J. Schwartz,<sup>8</sup> Y. Seino,<sup>55</sup> K. Senyo,<sup>79</sup> O. Seon,<sup>47</sup> M. E. Sevir,<sup>43</sup>  
V. Shebalin,<sup>5,57</sup> C. P. Shen,<sup>3</sup> T.-A. Shibata,<sup>74</sup> J.-G. Shiu,<sup>52</sup> B. Shwartz,<sup>5,57</sup> E. Solovieva,<sup>37,46</sup> S. Stanič,<sup>56</sup>  
M. Starič,<sup>27</sup> J. F. Strube,<sup>58</sup> J. Stypula,<sup>53</sup> T. Sumiyoshi,<sup>75</sup> M. Takizawa,<sup>62,17,60</sup> U. Tamponi,<sup>26,76</sup> F. Tenchini,<sup>43</sup>  
K. Trabelsi,<sup>16,12</sup> M. Uchida,<sup>74</sup> S. Uno,<sup>16,12</sup> Y. Ushiroda,<sup>16,12</sup> G. Varner,<sup>15</sup> A. Vinokurova,<sup>5,57</sup> V. Vorobyev,<sup>5,57</sup>  
A. Vossen,<sup>23</sup> C. H. Wang,<sup>51</sup> M.-Z. Wang,<sup>52</sup> P. Wang,<sup>24</sup> Y. Watanabe,<sup>28</sup> E. Widmann,<sup>64</sup> E. Won,<sup>34</sup>  
J. Yamaoka,<sup>58</sup> Y. Yamashita,<sup>54</sup> J. Yelton,<sup>10</sup> Z. P. Zhang,<sup>61</sup> V. Zhilich,<sup>5,57</sup> V. Zhukova,<sup>45</sup> and V. Zhulanov,<sup>5,57</sup>

(The Belle Collaboration)

<sup>1</sup>Aligarh Muslim University, Aligarh 202002

<sup>2</sup>University of the Basque Country UPV/EHU, 48080 Bilbao

<sup>3</sup>Beihang University, Beijing 100191

<sup>4</sup>University of Bonn, 53115 Bonn

<sup>5</sup>Budker Institute of Nuclear Physics SB RAS, Novosibirsk 630090

<sup>6</sup>Faculty of Mathematics and Physics, Charles University, 121 16 Prague

<sup>7</sup>Chonnam National University, Kwangju 660-701

<sup>8</sup>University of Cincinnati, Cincinnati, Ohio 45221

<sup>9</sup>Deutsches Elektronen-Synchrotron, 22607 Hamburg

<sup>10</sup>University of Florida, Gainesville, Florida 32611

<sup>11</sup>Justus-Liebig-Universität Gießen, 35392 Gießen

<sup>12</sup>SOKENDAI (The Graduate University for Advanced Studies), Hayama 240-0193

<sup>13</sup>Gyeongsang National University, Chinju 660-701

<sup>14</sup>Hanyang University, Seoul 133-791

<sup>15</sup>University of Hawaii, Honolulu, Hawaii 96822

<sup>16</sup>High Energy Accelerator Research Organization (KEK), Tsukuba 305-0801

<sup>17</sup>J-PARC Branch, KEK Theory Center, High Energy Accelerator Research Organization (KEK), Tsukuba 305-0801

<sup>18</sup>IKERBASQUE, Basque Foundation for Science, 48013 Bilbao

<sup>19</sup>Indian Institute of Science Education and Research Mohali, SAS Nagar, 140306

<sup>20</sup>Indian Institute of Technology Bhubaneswar, Satya Nagar 751007

<sup>21</sup>Indian Institute of Technology Guwahati, Assam 781039

<sup>22</sup>Indian Institute of Technology Madras, Chennai 600036

<sup>23</sup>Indiana University, Bloomington, Indiana 47408

<sup>24</sup>Institute of High Energy Physics, Chinese Academy of Sciences, Beijing 100049

<sup>25</sup>Institute of High Energy Physics, Vienna 1050

<sup>26</sup>INFN - Sezione di Torino, 10125 Torino

<sup>27</sup>J. Stefan Institute, 1000 Ljubljana

<sup>28</sup>Kanagawa University, Yokohama 221-8686

<sup>29</sup>Institut für Experimentelle Kernphysik, Karlsruher Institut für Technologie, 76131 Karlsruhe

<sup>30</sup>Kennesaw State University, Kennesaw, Georgia 30144

<sup>31</sup>King Abdulaziz City for Science and Technology, Riyadh 11442

<sup>32</sup>Department of Physics, Faculty of Science, King Abdulaziz University, Jeddah 21589

<sup>33</sup>Korea Institute of Science and Technology Information, Daejeon 305-806

- 58 <sup>34</sup>*Korea University, Seoul 136-713*  
59 <sup>35</sup>*Kyungpook National University, Daegu 702-701*  
60 <sup>36</sup>*École Polytechnique Fédérale de Lausanne (EPFL), Lausanne 1015*  
61 <sup>37</sup>*P.N. Lebedev Physical Institute of the Russian Academy of Sciences, Moscow 119991*  
62 <sup>38</sup>*Faculty of Mathematics and Physics, University of Ljubljana, 1000 Ljubljana*  
63 <sup>39</sup>*Ludwig Maximilians University, 80539 Munich*  
64 <sup>40</sup>*Luther College, Decorah, Iowa 52101*  
65 <sup>41</sup>*University of Maribor, 2000 Maribor*  
66 <sup>42</sup>*Max-Planck-Institut für Physik, 80805 München*  
67 <sup>43</sup>*School of Physics, University of Melbourne, Victoria 3010*  
68 <sup>44</sup>*University of Miyazaki, Miyazaki 889-2192*  
69 <sup>45</sup>*Moscow Physical Engineering Institute, Moscow 115409*  
70 <sup>46</sup>*Moscow Institute of Physics and Technology, Moscow Region 141700*  
71 <sup>47</sup>*Graduate School of Science, Nagoya University, Nagoya 464-8602*  
72 <sup>48</sup>*Kobayashi-Maskawa Institute, Nagoya University, Nagoya 464-8602*  
73 <sup>49</sup>*Nara Women's University, Nara 630-8506*  
74 <sup>50</sup>*National Central University, Chung-li 32054*  
75 <sup>51</sup>*National United University, Miao Li 36003*  
76 <sup>52</sup>*Department of Physics, National Taiwan University, Taipei 10617*  
77 <sup>53</sup>*H. Niewodniczanski Institute of Nuclear Physics, Krakow 31-342*  
78 <sup>54</sup>*Nippon Dental University, Niigata 951-8580*  
79 <sup>55</sup>*Niigata University, Niigata 950-2181*  
80 <sup>56</sup>*University of Nova Gorica, 5000 Nova Gorica*  
81 <sup>57</sup>*Novosibirsk State University, Novosibirsk 630090*  
82 <sup>58</sup>*Pacific Northwest National Laboratory, Richland, Washington 99352*  
83 <sup>59</sup>*University of Pittsburgh, Pittsburgh, Pennsylvania 15260*  
84 <sup>60</sup>*Theoretical Research Division, Nishina Center, RIKEN, Saitama 351-0198*  
85 <sup>61</sup>*University of Science and Technology of China, Hefei 230026*  
86 <sup>62</sup>*Showa Pharmaceutical University, Tokyo 194-8543*  
87 <sup>63</sup>*Soongsil University, Seoul 156-743*  
88 <sup>64</sup>*Stefan Meyer Institute for Subatomic Physics, Vienna 1090*  
89 <sup>65</sup>*Sungkyunkwan University, Suwon 440-746*  
90 <sup>66</sup>*School of Physics, University of Sydney, New South Wales 2006*  
91 <sup>67</sup>*Department of Physics, Faculty of Science, University of Tabuk, Tabuk 71451*  
92 <sup>68</sup>*Tata Institute of Fundamental Research, Mumbai 400005*  
93 <sup>69</sup>*Department of Physics, Technische Universität München, 85748 Garching*  
94 <sup>70</sup>*Toho University, Funabashi 274-8510*  
95 <sup>71</sup>*Department of Physics, Tohoku University, Sendai 980-8578*  
96 <sup>72</sup>*Earthquake Research Institute, University of Tokyo, Tokyo 113-0032*  
97 <sup>73</sup>*Department of Physics, University of Tokyo, Tokyo 113-0033*  
98 <sup>74</sup>*Tokyo Institute of Technology, Tokyo 152-8550*  
99 <sup>75</sup>*Tokyo Metropolitan University, Tokyo 192-0397*  
100 <sup>76</sup>*University of Torino, 10124 Torino*  
101 <sup>77</sup>*Virginia Polytechnic Institute and State University, Blacksburg, Virginia 24061*  
102 <sup>78</sup>*Wayne State University, Detroit, Michigan 48202*  
103 <sup>79</sup>*Yamagata University, Yamagata 990-8560*  
104 <sup>80</sup>*Yonsei University, Seoul 120-749*

We report the first observation of the radiative charm decay  $D^0 \rightarrow \rho^0 \gamma$  and the first search for  $CP$  violation in decays  $D^0 \rightarrow \rho^0 \gamma$ ,  $\phi \gamma$ , and  $\bar{K}^{*0}(892)\gamma$ , using a data sample of  $943 \text{ fb}^{-1}$  collected with the Belle detector at the KEKB asymmetric-energy  $e^+e^-$  collider. The branching fraction is measured to be  $\mathcal{B}(D^0 \rightarrow \rho^0 \gamma) = (1.77 \pm 0.30 \pm 0.07) \times 10^{-5}$ , where the first uncertainty is statistical and the second is systematic. The obtained  $CP$  asymmetries,  $\mathcal{A}_{CP}(D^0 \rightarrow \rho^0 \gamma) = +0.056 \pm 0.152 \pm 0.006$ ,  $\mathcal{A}_{CP}(D^0 \rightarrow \phi \gamma) = -0.094 \pm 0.066 \pm 0.001$ , and  $\mathcal{A}_{CP}(D^0 \rightarrow \bar{K}^{*0} \gamma) = -0.003 \pm 0.020 \pm 0.000$ , are consistent with no  $CP$  violation. We also present an improved measurement of the branching fractions  $\mathcal{B}(D^0 \rightarrow \phi \gamma) = (2.76 \pm 0.19 \pm 0.10) \times 10^{-5}$  and  $\mathcal{B}(D^0 \rightarrow \bar{K}^{*0} \gamma) = (4.66 \pm 0.21 \pm 0.21) \times 10^{-4}$ .

PACS numbers: 11.30.Er, 13.20.Fc, 13.25.Ft

Within the Standard Model (SM), charge-parity ( $CP$ ) matrix [1] and is expected to be very small for charmed violation in weak decays of hadrons arises due to a sin- hadrons: up to a few  $10^{-3}$  [2–4]. Observation of  $CP$  irreducible phase in the Cabibbo-Kobayashi-Maskawa violation above the SM expectation would be an indi-

cation of new physics. This phenomenon in the charm sector has been extensively probed in the past decade in many different decays [5], reaching a sensitivity below 0.1% in some cases [6]. The search for  $CP$  violation in radiative charm decays is complementary to the searches that have been exclusively performed in hadronic or leptonic decays. Theoretical calculations [7, 8] show that, in SM extensions with chromomagnetic dipole operators, sizable  $CP$  asymmetries can be expected in  $D^0 \rightarrow \phi\gamma$  and  $\rho^0\gamma$  decays. No experimental results exist to date regarding  $CP$  violation in any of the radiative  $D$  decays. Radiative charm decays are dominated by long-range non-perturbative processes that can enhance the branching fractions up to  $10^{-4}$ , whereas short-range interactions are predicted to yield rates at the level of  $10^{-8}$  [9, 10]. Measurements of branching fractions of these decays can therefore be used to test the QCD-based calculations of long-distance dynamics. The radiative decay  $D^0 \rightarrow \phi\gamma$  was first observed by Belle [11] and later measured with increased precision by BABAR [12]. In the same study, BABAR made the observation of  $D^0 \rightarrow \bar{K}^{*0}(892)\gamma$ . As for  $D^0 \rightarrow \rho^0\gamma$ , CLEO II has set an upper limit on its branching fraction at  $2 \times 10^{-4}$  [13].

In this Letter, we present the first observation of  $D^0 \rightarrow \rho^0\gamma$ , improved branching fraction measurements of  $D^0 \rightarrow \phi\gamma$  and  $\bar{K}^{*0}\gamma$ , as well as the first search for  $CP$  violation in all three decays. Inclusion of charge-conjugate modes is implied unless noted otherwise. The measurements are based on  $943 \text{ fb}^{-1}$  of data collected at or near the  $\Upsilon(nS)$  resonances ( $n = 2, 3, 4, 5$ ) with the Belle detector [14, 15], operating at the KEKB asymmetric-energy  $e^+e^-$  collider [16, 17]. The detector components relevant for our study are: a tracking system comprising a silicon vertex detector and a 50-layer central drift chamber (CDC), a particle identification (PID) system that consists of a barrel-like arrangement of time-of-flight scintillation counters (TOF) and an array of aerogel threshold Cherenkov counters (ACC), and a CsI(Tl) crystal-based electromagnetic calorimeter (ECL). All are located inside a superconducting solenoid coil that provides a 1.5 T magnetic field.

We use Monte Carlo (MC) events, generated using EVTGEN [18], JETSET [19] and PHOTOS [20], followed with a GEANT3 [21] based detector simulation, representing six times the data luminosity, to devise selection criteria and investigate possible sources of background. The selection optimization is performed by maximizing  $S/\sqrt{S+B}$ , where  $S$  ( $B$ ) is the number of signal (background) events in a signal window of the reconstructed  $D^0$  invariant mass  $1.8 \text{ GeV}/c^2 < M(D^0) < 1.9 \text{ GeV}/c^2$ . The branching fraction of  $D^0 \rightarrow \rho^0\gamma$  is set to  $3 \times 10^{-5}$  in simulations in accordance with Ref. [7], while the branching fractions of the other two decay modes are set to their world-average values [22].

We reconstruct  $D^0$  mesons by combining a  $\rho^0$ ,  $\phi$ , or a  $\bar{K}^{*0}$  with a photon. The vector resonances are formed

from  $\pi^+\pi^-$  ( $\rho^0$ ),  $K^+K^-$  ( $\phi$ ), and  $K^-\pi^+$  ( $\bar{K}^{*0}$ ) combinations. Charged particles are reconstructed in the tracking system. A likelihood ratio for a given track to be a kaon or pion is obtained by utilizing specific ionization in the CDC, light yield from the ACC, and information from the TOF. Photons are detected with the ECL and required to have energies of at least 540 MeV. To suppress events with two daughter photons from a  $\pi^0$  decay forming a merged cluster, we restrict the ratio of the energy deposited in a  $3 \times 3$  array of ECL crystals ( $E_9$ ) and that in the enclosing  $5 \times 5$  array ( $E_{25}$ ) to be above 0.94. About 63% of merged clusters are rejected by this requirement. We retain candidate  $\rho^0$ ,  $\phi$ , or  $\bar{K}^{*0}$  resonances if their invariant masses are within 150, 11, or 60  $\text{MeV}/c^2$  of their nominal masses [22], respectively. The  $D^0$  mesons are required to originate from  $D^{*+} \rightarrow D^0\pi^+$  in order to identify the  $D^0$  flavor and to suppress the combinatorial background. The associated track must satisfy the aforementioned pion-hypothesis requirement. The  $D^0$  daughters are refitted to a common vertex, and the resulting  $D^0$  and the slow pion candidate from  $D^{*+}$  decay are constrained to originate from a common point within the interaction point region. Confidence levels exceeding  $10^{-3}$  are required for both fits. To suppress combinatorial background, we restrict the energy released in the decay,  $q \equiv M(D^{*+}) - M(D^0) - m(\pi^+)$ , where  $m$  is the nominal mass, to lie in a  $\pm 0.6 \text{ MeV}/c^2$  window around the nominal value [22]. To further reduce the combinatorial background contribution, we require the momentum of the  $D^{*+}$  in the center-of-mass system [ $p_{\text{CMS}}(D^{*+})$ ] to exceed 2.72, 2.42, and 2.17  $\text{GeV}/c$  in the  $\rho^0\gamma$ ,  $\phi\gamma$ , and  $\bar{K}^{*0}\gamma$  modes, respectively.

We measure the branching fractions and  $CP$  asymmetries of aforementioned radiative decays relative to well-measured hadronic  $D^0$  decays to  $\pi^+\pi^-$ ,  $K^+K^-$ , and  $K^-\pi^+$  for the  $\rho^0$ ,  $\phi$ , and  $\bar{K}^{*0}$  mode, respectively. The signal branching fraction is

$$\mathcal{B}_{\text{sig}} = \mathcal{B}_{\text{norm}} \times \frac{N_{\text{sig}}}{N_{\text{norm}}} \times \frac{\varepsilon_{\text{norm}}}{\varepsilon_{\text{sig}}}, \quad (1)$$

where  $N$  is the extracted yield,  $\varepsilon$  the reconstruction efficiency, and  $\mathcal{B}$  the branching fraction for the corresponding mode. The raw asymmetry in decays of  $D^0$  mesons to a specific final state  $f$ ,

$$A_{\text{raw}} = \frac{N(D^0 \rightarrow f) - N(\bar{D}^0 \rightarrow \bar{f})}{N(D^0 \rightarrow f) + N(\bar{D}^0 \rightarrow \bar{f})}, \quad (2)$$

depends not only on the  $CP$  asymmetry,  $\mathcal{A}_{CP} = [\mathcal{B}(D^0 \rightarrow f) - \mathcal{B}(\bar{D}^0 \rightarrow \bar{f})]/[\mathcal{B}(D^0 \rightarrow f) + \mathcal{B}(\bar{D}^0 \rightarrow \bar{f})]$ , but also on the contributions from the forward-backward production asymmetry ( $A_{\text{FB}}$ ) [23–25] and the asymmetry due to different reconstruction efficiencies for positively and negatively charged particles ( $A_{\varepsilon}^{\pm}$ ):  $A_{\text{raw}} = \mathcal{A}_{CP} + A_{\text{FB}} + A_{\varepsilon}^{\pm}$ . Here, we have used a linear approximation assuming all terms to be small. The last two

217 terms can be eliminated using the same normalization  
218 mode as used in the branching fraction measurements:

$$\mathcal{A}_{CP}^{\text{sig}} = A_{\text{raw}}^{\text{sig}} - A_{\text{raw}}^{\text{norm}} + \mathcal{A}_{CP}^{\text{norm}}, \quad (3)$$

219 where  $\mathcal{A}_{CP}^{\text{norm}}$  is the nominal value of  $CP$  asymmetry of  
220 the normalization mode [5].

221 The dominant background arises from  $D^0 \rightarrow f^+ f^- \pi^0$   
222 decays, with the  $\pi^0$  subsequently decaying to a pair of  
223 photons, e.g.,  $D^0 \rightarrow \phi \pi^0 (\rightarrow \gamma\gamma)$ . If one of the daughter  
224 photons is missed in the reconstruction, the final state  
225 mimics the signal decay. Such events are suppressed with  
226 a dedicated  $\pi^0$  veto in the form of a neural network [26]  
227 constructed from two mass-veto variables, described be-  
228 low. The signal photon is paired for the first (second)  
229 time with all other photons in the event having an en-  
230 ergy greater than 30 (75) MeV. The pair in each set whose  
231 diphoton invariant mass lies closest to  $m(\pi^0)$  is fed to the  
232 network. The final criterion on the veto variable rejects  
233 about 60% of background while retaining 85% of signal.  
234 With this method, we reject 13% more background at  
235 the same signal efficiency as compared to the veto used  
236 in previous Belle analyses [27]. A similar veto is con-  
237 sidered for background from  $\eta \rightarrow \gamma\gamma$ , but is found to  
238 be ineffective due to the larger  $\eta$  mass, which shifts the  
239 background further away from the signal peak.

240 We extract the signal yield and  $CP$  asymmetry via  
241 a simultaneous unbinned extended maximum likelihood  
242 fit of  $D^0$  and  $\bar{D}^0$  samples to the invariant mass of the  
243  $D^0$  candidates and the cosine of the helicity angle  $\theta_H$ .  
244 The latter is the angle between the momenta of the  $D^0$   
245 and the  $\pi^+$ ,  $K^+$ , or  $K^-$  in the rest frame of the  $\rho^0$ ,  $\phi$ ,  
246 or  $\bar{K}^{*0}$ , respectively. By angular momentum conserva-  
247 tion, the signal  $\cos\theta_H$  distribution depicts a  $1 - \cos^2\theta_H$   
248 dependence; no background contribution is expected to  
249 exhibit a similar shape. For the  $\rho^0$  and  $\bar{K}^{*0}$  modes, we  
250 restrict the helicity angle range to  $-0.8 < \cos\theta_H < 0.4$  to  
251 suppress backgrounds that peak at the edges of the dis-  
252 tribution. For the  $\phi$  mode, where the background levels  
253 are lower overall, the entire  $\cos\theta_H$  range is used. The  $D^0$   
254 candidate mass is restricted to  $1.67 \text{ GeV}/c^2 < M(D^0) <$   
255  $2.06 \text{ GeV}/c^2$  for all three signal channels.

256 The invariant mass distribution of signal events is mod-  
257 eled with a Crystal-Ball probability density function [28]  
258 (PDF) for the  $\rho^0$  and  $\phi$  modes, and with the sum of a  
259 Crystal-Ball and two Gaussians for the  $\bar{K}^{*0}$  mode. To  
260 take into account possible differences between MC and  
261 data, a free offset and scale factor are implemented for  
262 the mean and width of the  $\bar{K}^{*0}$  PDF, respectively. The  
263 obtained values are applied to the other two modes.

264 The  $\pi^0$ - and  $\eta$ -type background  $M(D^0)$  distributions  
265 are described with a pure Crystal-Ball or the sum of ei-  
266 ther a Crystal-Ball or logarithmic Gaussian [29] and up  
267 to two additional Gaussians. For the  $\rho^0$  mode, the  $\pi^0$ -  
268 type backgrounds are  $\rho^0\pi^0$ ,  $\rho^\pm\pi^\mp$  and  $K^-\rho^+$  with the  
269 kaon being misidentified as pion. For the  $\phi$  mode, the  
270 only  $\pi^0$ -type background is the decay  $D^0 \rightarrow \phi\pi^0$ . For

271 the  $\bar{K}^{*0}$  mode, the  $\pi^0$ - and  $\eta$ -type backgrounds are the  
272 decays  $D^0 \rightarrow \bar{K}^{*0}\pi^0$ ,  $K^-\rho^+$ ,  $K_0^*(1430)^-\pi^+$ ,  $K^{*-}\pi^+$ ,  
273 nonresonant  $K^-\pi^+\pi^0$ ,  $\bar{K}^{*0}\eta$  and nonresonant  $K^-\pi^+\eta$ .  
274 In all three signal modes, the ‘other- $D^0$ ’ background com-  
275 prises all other decays wherein the  $D^0$  is reconstructed  
276 from the majority of daughter particles. In the  $\rho^0$   
277 ( $\bar{K}^{*0}$ ) mode, there are two additional small backgrounds:  
278  $\pi^+\pi^-(K^-\pi^+)$  with the photon being emitted as final  
279 state radiation (FSR), and  $K^-\rho^+$  with the photon aris-  
280 ing from the radiative decay of the charged  $\rho$  meson. As  
281 there are no missing particles, these decays exhibit the  
282 same  $M(D^0)$  distribution as the signal decays. We jointly  
283 denote them as irreducible background. Their yields are  
284 fixed to MC expectations and the known branching frac-  
285 tions [22]. The remaining combinatorial background is  
286 parametrized in  $M(D^0)$  with an exponential function in  
287 the  $\phi$  mode and a second-order Chebyshev polynomial  
288 in the  $\rho^0$  and  $\bar{K}^{*0}$  modes. All parameters describing the  
289 combinatorial background are allowed to vary in the fit.  
290 Possible correlations among the fit variables are negli-  
291 gible, except for the  $\bar{K}^{*0}\pi^0$  and  $K^-\rho^+$  backgrounds in  
292 the  $\bar{K}^{*0}$  mode that are accomodated with an additional  
293 Gaussian in the mass PDF whose relative contribution is  
294 a function of  $\cos\theta_H$ .

295 The  $M(D^0)$  PDF shape for the  $\pi^0(\eta)$ -type background,  
296 obtained from MC samples, is calibrated using the forbid-  
297 den decay  $D^0 \rightarrow K_S^0\gamma$ , which yields mostly background  
298 from  $D^0 \rightarrow K_S^0\pi^0$  and  $D^0 \rightarrow K_S^0\eta$ . The same PID cri-  
299 teria as for signal decays are applied, along with the  $q$   
300 and  $p_{\text{CMS}}(D^{*+})$  requirements as determined for the  $\phi$   
301 mode. The  $K_S^0 \rightarrow \pi^+\pi^-$  candidates in a  $\pm 9 \text{ MeV}/c^2$   
302 window around the nominal mass are accepted. To cali-  
303 brate the distribution, the simulated shape is smeared  
304 with a Gaussian function of width  $(7 \pm 1) \text{ MeV}/c^2$  and  
305 an offset  $(-1.33 \pm 0.25) \text{ MeV}/c^2$ .

306 The  $\cos\theta_H$  signal distribution is parametrized as  $1 -$   
307  $\cos^2\theta_H$  for all three modes. For the  $V\pi^0$  and  $V\eta$  ( $V =$   
308  $\rho^0, \phi, \bar{K}^{*0}$ ) categories, the shape is close to  $\cos^2\theta_H$  and  
309 described with a second- ( $\rho^0$  and  $\phi$  mode) or third-order  
310 ( $\bar{K}^{*0}$  mode) Chebyshev polynomial. In the  $\phi$  mode, a  
311 linear term in  $\cos\theta_H$  is added with a free coefficient to  
312 take into account possible interference between resonant  
313 and nonresonant amplitudes. For other background cate-  
314 gories, the distributions are modeled using suitable PDFs  
315 based on MC predictions.

316 Apart from normalizations, the asymmetries  $A_{\text{raw}}$  of  
317 signal and background modes are left free in the fit. All  
318 PDF shapes are fixed to MC values, unless previously  
319 stated otherwise.

320 In the  $\bar{K}^{*0}$  mode, the yields (and  $A_{\text{raw}}$ ) of certain  
321 backgrounds that contain a small number of events (one  
322 or two orders of magnitude less than signal) are fixed:  
323  $K_0^*(1430)^-\pi^+$ ,  $K^{*-}\pi^+$ , and the ‘other- $D^0$ ’ background.  
324 The same is done for backgrounds with a photon from  
325 FSR or radiative  $\rho$  decay in the  $\rho^0$  and  $\bar{K}^{*0}$  modes. All  
326 fixed yields are scaled by the ratio between reconstructed

Table I. Efficiencies, extracted yields and  $A_{\text{raw}}$  values for all signal and normalization modes. The uncertainties are statistical.

	Efficiency [%]	Yield	$A_{\text{raw}}$
$\rho^0\gamma$	$6.77 \pm 0.09$	$500 \pm 85$	$+0.064 \pm 0.152$
$\phi\gamma$	$9.77 \pm 0.10$	$524 \pm 35$	$-0.091 \pm 0.066$
$\bar{K}^{*0}\gamma$	$7.81 \pm 0.03$	$9104 \pm 396$	$-0.002 \pm 0.020$
$\pi^+\pi^-$	$21.4 \pm 0.12$	$(1.28 \pm 0.01) \times 10^5$	$(8.1 \pm 3.0) \times 10^{-3}$
$K^+K^-$	$22.7 \pm 0.12$	$(3.62 \pm 0.01) \times 10^5$	$(2.2 \pm 1.7) \times 10^{-3}$
$K^-\pi^+$	$27.0 \pm 0.13$	$(4.02 \pm 0.02) \times 10^6$	$(1.3 \pm 0.5) \times 10^{-3}$

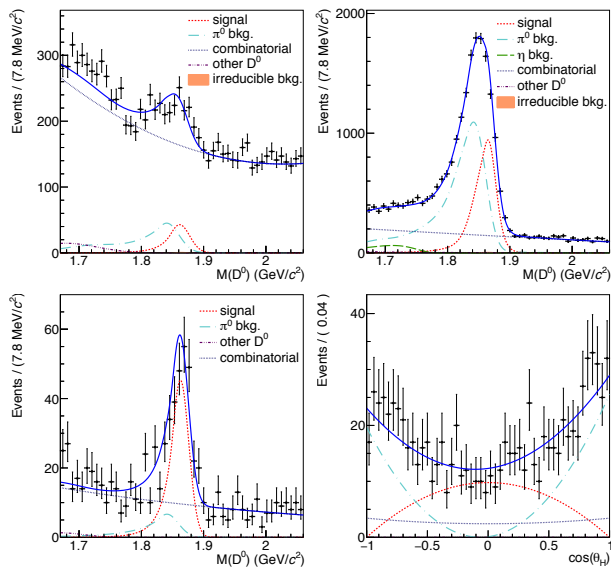


Figure 1. Top two panels are signal-enhanced projections of the combined  $M(D^0)$  distribution for  $D^0 \rightarrow \rho^0\gamma$  (left) and  $\bar{K}^{*0}\gamma$  (right). Bottom two panels are the signal-enhanced  $M(D^0)$  (left) and  $\cos\theta_H$  (right) distributions for  $D^0 \rightarrow \phi\gamma$ . Fit results are superimposed, with the fit components identified in the panel legend.

signal events in data and simulation of the normalization modes. We impose an additional constraint in the  $\bar{K}^{*0}$  mode by assigning two common  $A_{\text{raw}}$  variables to  $\pi^0$ - and  $\eta$ -type backgrounds, respectively. Since all are Cabibbo-favored decays,  $\mathcal{A}_{CP}$  is expected to be zero, while other asymmetries contributing to  $A_{\text{raw}}$  are the same for decays with the same final-state particles.

Fig. 1 shows the signal-enhanced  $M(D^0)$  projections of the combined sample in the region  $-0.3 < \cos\theta_H < 0.3$  for all three signal modes, as well as the signal-enhanced  $\cos\theta_H$  projection in the  $1.85 \text{ GeV}/c^2 < M(D^0) < 1.88 \text{ GeV}/c^2$  region for the  $\phi\gamma$  mode [30]. The obtained signal yields and raw asymmetries are listed in Table I, along with reconstruction efficiencies. The background raw asymmetries are consistent with zero.

The analysis of the normalization modes relies on the previous analysis by Belle [31]. The same selection criteria as for signal modes for PID, vertex fit,  $q$  and

$p_{\text{CMS}}(D^{*+})$  are applied. The signal yield is extracted by subtracting the background in a signal window of  $M(D^0)$ , where the background is estimated from a symmetrical upper and lower sideband. The signal window and sidebands for the  $\pi^+\pi^-$  mode are  $\pm 15 \text{ MeV}/c^2$  and  $\pm(20\text{-}35) \text{ MeV}/c^2$  around the nominal value [22], respectively. For the  $K^+K^-$  mode, the signal window is  $\pm 14 \text{ MeV}/c^2$  and sidebands are  $\pm(31\text{-}45) \text{ MeV}/c^2$ , whereas for the  $K^-\pi^+$  mode, the signal window is  $\pm 16.2 \text{ MeV}/c^2$  and sidebands are  $\pm(28.8\text{-}45.0) \text{ MeV}/c^2$ . The obtained signal yields and raw asymmetries are also listed in Table I.

The systematic uncertainties are listed in Table II. All uncertainties are simultaneously estimated for  $\mathcal{B}$  and  $\mathcal{A}_{CP}$ , unless stated otherwise. There are two main sources: those due to the selection criteria and those arising from the signal extraction method, both for signal and normalization modes. Some of the uncertainties from the first group cancel if they are common to the signal and respective normalization mode, such as those related to PID, vertex fit, and the requirement on  $p_{\text{CMS}}(D^{*+})$ . A 2.2% uncertainty is ascribed to photon reconstruction efficiency [32]. Due to the presence of the photon in the signal modes, the resolution of the  $q$  distribution is worse than in the normalization modes. Thus, the related uncertainties cannot be assumed to cancel completely. We separately estimate the uncertainty due to the  $q$  requirement using the control channel  $D^0 \rightarrow \bar{K}^{*0}\pi^0$ . For both MC and data, the efficiency is estimated by calculating the ratio  $R$  of the signal yield, extracted with and without the requirement on  $q$ . Then, the double ratio  $R_{\text{MC}}/R_{\text{data}}$  is calculated to assess the possible difference between simulation and data. We obtain  $R_{\text{MC}}/R_{\text{data}}(q) = 1.0100 \pm 0.0016$ . We do not correct the efficiency by the central value; instead, we assign a systematic uncertainty of 1.16%.

The double-ratio method is also used to estimate the uncertainty due to the  $\pi^0$ -veto requirement on the control channel  $D^0 \rightarrow K_S^0\pi^0$ . The veto is calculated by pairing the first daughter photon (the more energetic one) of the  $\pi^0$  with all others, but for the second daughter. The ratio  $R$  of so-discarded events is calculated for MC and data, with all other selection criteria applied. The obtained double ratio is  $R_{\text{MC}}/R_{\text{data}}(\pi^0 \text{ veto}) = 1.002 \pm 0.005$ . The error directly translates to the systematic uncertainty of the efficiency.

The systematic uncertainties due to the  $E_9/E_{25}$  and  $E_\gamma$  requirements are estimated on the  $\bar{K}^{*0}$  mode by repeating the fit without any constraint on the variable in question. The systematic error is the difference between the central value of the ratio  $N_{\text{sig}}/\varepsilon_{\text{sig}}$  from this fit and that of the nominal fit. The obtained uncertainties are 0.23% for  $E_9/E_{25}$  and 1.15% for  $E_\gamma$ .

The systematic uncertainties due to the requirement on the mass of the vector meson are estimated using the mass distribution, modeled with a relativistic Breit-Wigner function. In the signal window, we compare the

integrals of the nominal function and the same modified by the uncertainties on the central value and width. The obtained uncertainties are 0.2% for the  $\rho^0$  mode, 0.1% for the  $\phi$  mode, and 1.7% for the  $\bar{K}^{*0}$  mode. All uncertainties described above are summed in quadrature and the final value is listed as ‘Efficiency’ in Table II. They affect only the branching fraction, as they cancel in Eq. 2.

For the fit procedure, a systematic uncertainty must be ascribed to every parameter that is determined and fixed to MC values but might differ in data. The fit procedure is repeated with each parameter varied by its uncertainty on the positive and negative sides. The larger deviation from the nominal branching fraction or  $\mathcal{A}_{CP}$  value is taken as the double-sided systematic error and these are summed in quadrature for all parameters. An uncertainty is assigned to the calibration offset and width of the  $\pi^0$ -type backgrounds. For the  $\phi$  and  $\rho^0$  modes, the uncertainty is calculated for the width scale factor (and offset) of the signal  $M(D^0)$  PDF and  $\pi^0$ -type background varied simultaneously. All these quadratically summed uncertainties are listed as ‘Fit parametrization’ in Table II.

The values of the fixed yields of some backgrounds in the  $\rho^0$  and  $\bar{K}^{*0}$  mode are varied according to the uncertainties of the respective branching fractions [22]. For the category with the FSR photon, a 20% variation is used [33]. As the branching fractions contributing to the ‘other- $D^0$ ’ background in the  $\bar{K}^{*0}$  mode are unknown, we apply the largest variation from among other categories. The quadratically summed uncertainty is listed as ‘Background normalization’ in Table II.

For the normalization modes, the procedure is repeated with shifted sidebands, starting from  $\pm 25 \text{ MeV}/c^2$  from the nominal  $m(D^0)$  value. The statistical error from sideband subtraction is taken into account. Since possible differences in the signal shape between simulation and data could also affect the signal yield, a similar procedure as for the calibration of the  $\pi^0$  background is performed. A systematic uncertainty is assigned for the case when the MC shape is smeared by a Gaussian of width  $1.6 \text{ MeV}/c^2$ . All uncertainties arising from normalization modes are summed in quadrature and listed as ‘Normalization mode’ in Table II.

Finally, an uncertainty is assigned by varying the nominal values of the branching fractions and  $\mathcal{A}_{CP}$  of the normalization modes and vector meson sub-decay modes by their respective uncertainties.

We have conducted a measurement of the branching fraction and  $\mathcal{A}_{CP}$  in three radiative charm decays  $D^0 \rightarrow \rho^0\gamma$ ,  $\phi\gamma$ , and  $\bar{K}^{*0}\gamma$  using the full dataset recorded by the Belle experiment. We report the first observation of  $D^0 \rightarrow \rho^0\gamma$  with a significance of  $5.5\sigma$ , including systematic uncertainties. The significance is calculated as  $\sqrt{-2\ln(\mathcal{L}_0/\mathcal{L}_{\max})}$ , where  $\mathcal{L}_0$  is the likelihood value with the signal yield fixed to zero and  $\mathcal{L}_{\max}$  is that of the nominal fit. The systematic uncertainties are in-

Table II. Systematic uncertainties for all three signal modes.

	$\sigma(\mathcal{B})/\mathcal{B}$ [%]			$\mathcal{A}_{CP}$ [ $\times 10^{-3}$ ]		
	$\phi$	$\bar{K}^{*0}$	$\rho^0$	$\phi$	$\bar{K}^{*0}$	$\rho^0$
Efficiency	2.8	3.3	2.8	–	–	–
Fit parametrization	1.0	2.8	2.3	0.1	0.4	5.3
Background normalization	–	0.3	0.6	–	0.2	0.5
Normalization mode	0.0	0.0	0.1	0.5	0.0	0.3
External $\mathcal{B}$ and $\mathcal{A}_{CP}$	2.0	1.0	1.8	1.2	0.0	1.5
Total	3.6	4.5	4.1	1.3	0.4	5.5

cluded by convolving the statistical likelihood function with a Gaussian of width equal to the systematic uncertainty that affects the signal yield. The measured ratios of branching fractions to their normalization modes are  $(1.25 \pm 0.21 \pm 0.05) \times 10^{-2}$ ,  $(6.88 \pm 0.47 \pm 0.21) \times 10^{-3}$  and  $(1.19 \pm 0.05 \pm 0.05) \times 10^{-2}$  for  $D^0 \rightarrow \rho^0\gamma$ ,  $\phi\gamma$ , and  $\bar{K}^{*0}\gamma$ , respectively. The first uncertainty is statistical and the second systematic. Using world-average values for the normalization modes [22], we obtain

$$\begin{aligned} \mathcal{B}(D^0 \rightarrow \rho^0\gamma) &= (1.77 \pm 0.30 \pm 0.07) \times 10^{-5}, \\ \mathcal{B}(D^0 \rightarrow \phi\gamma) &= (2.76 \pm 0.19 \pm 0.10) \times 10^{-5}, \\ \mathcal{B}(D^0 \rightarrow \bar{K}^{*0}\gamma) &= (4.66 \pm 0.21 \pm 0.21) \times 10^{-4}. \end{aligned}$$

For the  $\rho^0$  mode, the obtained value is considerably larger than theoretical expectations [34, 35]. The result of the  $\phi$  mode is improved compared to the previous determinations by Belle and BABAR, and is consistent with the world average value [22]. Our branching fraction of the  $\bar{K}^{*0}$  mode is  $3.3\sigma$  above the BABAR measurement [12]. Both  $\phi$  and  $\bar{K}^{*0}$  results agree with the latest theoretical calculations [10].

We also report the first measurement of  $\mathcal{A}_{CP}$  in these decays. The values, obtained from Eq. 3:

$$\begin{aligned} \mathcal{A}_{CP}(D^0 \rightarrow \rho^0\gamma) &= +0.056 \pm 0.152 \pm 0.006, \\ \mathcal{A}_{CP}(D^0 \rightarrow \phi\gamma) &= -0.094 \pm 0.066 \pm 0.001, \\ \mathcal{A}_{CP}(D^0 \rightarrow \bar{K}^{*0}\gamma) &= -0.003 \pm 0.020 \pm 0.000, \end{aligned}$$

are consistent with no  $CP$  violation. Since the uncertainty is statistically dominated, the sensitivity can be greatly enhanced at the upcoming Belle II experiment [36].

We thank the KEKB group for excellent operation of the accelerator; the KEK cryogenics group for efficient solenoid operations; and the KEK computer group, the NII, and PNNL/EMSL for valuable computing and SINET4 network support. We acknowledge support from MEXT, JSPS and Nagoya’s TLPRC (Japan); ARC (Australia); FWF (Austria); NSFC and CCEPP (China);

- 487 MSMT (Czechia); CZF, DFG, EXC153, and VS (Ger-  
488 many); DST (India); INFN (Italy); MOE, MSIP, NRF,  
489 BK21Plus, WCU and RSRI (Korea); MNiSW and NCN  
490 (Poland); MES and RFAAE (Russia); ARRS (Slovenia);  
491 IKERBASQUE and UPV/EHU (Spain); SNSF (Switzer-  
492 land); MOE and MOST (Taiwan); and DOE and NSF  
493 (USA).
- 
- 494 [1] M. Kobayashi and T. Maskawa, *Prog. Theor. Phys.* **49**,  
495 652 (1973).  
496 [2] I. I. Bigi, A. Paul, and S. Recksiegel, *JHEP* **06**, 089  
497 (2011), arXiv:1103.5785 [hep-ph].  
498 [3] G. Isidori, J. F. Kamenik, Z. Ligeti, and G. Perez, *Phys.*  
499 *Lett. B* **711**, 46 (2012), arXiv:1111.4987 [hep-ph].  
500 [4] J. Brod, A. L. Kagan, and J. Zupan, *Phys. Rev. D* **86**,  
501 014023 (2012), arXiv:1111.5000 [hep-ph].  
502 [5] Y. Amhis *et al.* (Heavy Flavor Averaging Group  
503 (HFAG)), (2014), arXiv:1412.7515 [hep-ex].  
504 [6] R. Aaij *et al.* (LHCb Collaboration), *Phys. Rev. Lett.*  
505 **116**, 191601 (2016), arXiv:1602.03160 [hep-ex].  
506 [7] G. Isidori and J. F. Kamenik, *Phys. Rev. Lett.* **109**,  
507 171801 (2012), arXiv:1205.3164 [hep-ph].  
508 [8] J. Lyon and R. Zwicky, (2012), arXiv:1210.6546 [hep-ph].  
509 [9] G. Burdman, E. Golowich, J. L. Hewett, and S. Pakvasa,  
510 *Phys. Rev. D* **52**, 6383 (1995), arXiv:hep-ph/9502329  
511 [hep-ph].  
512 [10] S. Fajfer, in *Proceedings of CHARM-2015*, edited by  
513 A. A. Petrov *et al.* (SLAC Electronic Proceedings, 2015)  
514 arXiv:1509.01997 [hep-ph].  
515 [11] O. Tajima *et al.* (Belle Collaboration), *Phys. Rev. Lett.*  
516 **92**, 101803 (2004).  
517 [12] B. Aubert *et al.* (BaBar Collaboration), *Phys. Rev. D*  
518 **78**, 071101(R) (2008), arXiv:0808.1838 [hep-ex].  
519 [13] D. M. Asner *et al.* (CLEO Collaboration), *Phys. Rev. D*  
520 **58**, 092001 (1998), arXiv:hep-ex/9803022 [hep-ex].  
521 [14] A. Abashian *et al.*, *Nucl. Instrum. Method Phys. Res.,*  
522 *Sect. A* **479**, 117 (2002).  
523 [15] J. Brodzicka *et al.* (Belle Collaboration), *PTEP* **2012**,  
524 04D001 (2012), arXiv:1212.5342 [hep-ex].  
525 [16] S. Kurokawa and E. Kikutani, *Nucl. Instrum. Method*  
526 *Phys. Res., Sect. A* **499**, 1 (2003).  
527 [17] T. Abe *et al.*, *PTEP* **2013**, 03A001 (2013).  
528 [18] D. J. Lange, *Nucl. Instrum. Method Phys. Res., Sect. A*  
529 **462**, 152 (2001).  
530 [19] T. Sjostrand, *Comput. Phys. Commun.* **82**, 74 (1994).  
531 [20] P. Golonka and Z. Was, *Eur. Phys. J. C* **45**, 97 (2006),  
532 arXiv:hep-ph/0506026 [hep-ph].  
533 [21] R. Brun, F. Bruyant, M. Maire, A. C. McPherson, and  
534 P. Zancarini, (1987).  
535 [22] K. A. Olive *et al.* (Particle Data Group), *Chin. Phys. C*  
536 **38**, 090001 (2014).  
537 [23] F. A. Berends, K. J. F. Gaemers, and R. Gastmans,  
538 *Nucl. Phys. B* **63**, 381 (1973).  
539 [24] R. W. Brown, K. O. Mikaelian, V. K. Cung, and E. A.  
540 Paschos, *Phys. Lett. B* **43**, 403 (1973).  
541 [25] R. J. Cashmore, C. M. Hawkes, B. W. Lynn, and R. G.  
542 Stuart, *Z. Phys. C* **30**, 125 (1986).  
543 [26] M. Feindt and U. Kerzel, *Nucl. Instrum. Method Phys.*  
544 *Res., Sect. A* **559**, 190 (2006).  
545 [27] P. Koppenburg *et al.* (Belle Collaboration), *Phys. Rev.*  
546 *Lett.* **93**, 061803 (2004), arXiv:hep-ex/0403004 [hep-ex].  
547 [28] T. Skwarnicki, Ph.D. thesis, Cracow, INP (1986).  
548 [29] H. Ikeda *et al.* (Belle Collaboration), *Nucl. Instrum.*  
549 *Method Phys. Res., Sect. A* **441**, 401 (2000).  
550 [30] See Supplemental Material at [URL will be inserted by  
551 publisher] for projections to both fit variables for both  
552  $D^0$  flavours, for all three signal channels.  
553 [31] M. Staric *et al.* (Belle Collaboration), *Phys. Lett. B* **670**,  
554 190 (2008), arXiv:0807.0148 [hep-ex].  
555 [32] N. K. Nisar *et al.* (Belle Collaboration), *Phys. Rev. D*  
556 **93**, 051102(R) (2016), arXiv:1512.02992 [hep-ex].  
557 [33] M. Benayoun, S. I. Eidelman, V. N. Ivanchenko, and  
558 Z. K. Silagadze, *Mod. Phys. Lett. A* **14**, 2605 (1999),  
559 arXiv:hep-ph/9910523 [hep-ph].  
560 [34] A. Khodjamirian, G. Stoll, and D. Wyler, *Phys. Lett. B*  
561 **358**, 129 (1995), arXiv:hep-ph/9506242 [hep-ph].  
562 [35] S. Fajfer, S. Prelovsek, and P. Singer, *Eur. Phys. J. C*  
563 **6**, 471 (1999), arXiv:hep-ph/9801279 [hep-ph].  
564 [36] T. Abe *et al.* (Belle II Collaboration), (2010),  
565 arXiv:1011.0352 [physics.ins-det].